Journal of Photochemistry & Photobiology A: Chemistry 371 (2019) 10–16

Contents lists available at ScienceDirect

Journal of Photochemistry & Photobiology A: Chemistry

journal homepage: www.elsevier.com/locate/jphotochem

Highly colloidal luminescent porous Tb-doped gadolinium oxide nanoparticles: Photophysical and luminescent properties

Anees A. Ansari[a,*], Naushad Ahmad[b], Joselito P. Labis[a]

[a] King Abdullah Institute for Nanotechnology, King Saud University, Riyadh, 11451, Saudi Arabia
[b] Department of Chemistry, King Saud University, Riyadh, 11451, Saudi Arabia

ARTICLE INFO

Keywords:
$Gd_2O_3Tb^{3+}$ nanoparticles
Solubility
Optical properties
zeta potential
Luminescence properties

ABSTRACT

Highly colloidal luminescent Gd_2O_3:Tb nanoparticles(NPs) were prepared by urea-based homogeneous co-precipitation process. X-ray diffraction pattern (XRD), transmission electron microscopy(TEM), energy dispersive x-ray analysis(EDX), thermogravimetric analysis(TGA), zeta potential, Fourier transform infrared(FTIR), FT-Raman, UV/Visible and photoluminescence spectroscopy to examine the crystallographic, phase purity, shape & size, thermal stability, surface chemistry, optical and photoluminescence properties. XRD results exhibited the single phase, highly pure cubic phase Gd_2O_3:Tb nanocrystals with an average grain size of 10–20 nm. The Gd_2O_3:Tb NPs exhibits attractive thermal, optical and luminescent properties for their use in long-term biological studies because of high thermal, photo-stability and strong emission sensitivities in the visible region. Optical features of Gd_2O_3:Tb NPs were examined in aqueous media and estimated energy band gap on the basis of absorption spectra. An observed strong peak located at 359 cm^{-1} is assigned to the F_g Raman active mode of cubic phase of nanocrystalline Gd_2O_3. The luminescence spectra show well dominant green emission transition in between 535–560 nm ($^5D_4 \rightarrow {}^7F_5$) under monitoring UV light (325 nm). Optically active, aqueous sensitivities, porous surface and strong luminescent NPs as revealed from TEM micrographs could be a promising candidate for future fluorescent biomedical applications.

1. Introduction

Along with the rapid development in nanotechnology, most intensive research activities have been focused on luminescent nanomaterials [1–5]. Luminescent nanomaterials are most promising because of their diversified applications in the different field of applied material and biomedical sciences such as solar cells, laser, penal display, optical diode, bio-photonic, photodynamic therapy, biolabeling/optical bio-probe and drug delivery etc [6–21]. Up to now various luminescent nanomaterials have been applied for this diversified material and biomedical applications such as quantum dots, plasmonic nanoparticles, silica, and organic dyes etc [3,22–24]. However, they are not photochemically stable, narrow absorption, broad emission transition, auto-fluorescence and allow short observation time because of their easy photo-bleaching. In order to resolve this problem, various lanthanide nanomaterials have been applied for applied biomedical sciences, due to their high photo-chemical thermal stability, bright photo-luminescence, large Stocke's shift, less auto-fluorescence, narrow absorption and emission lines in the visible region, good biocompatibility and less toxic nature [10,25–27]. Among the rare-earth nanomaterials family, gadolinium oxide (Gd_2O_3) and yttrium oxide (Y_2O_3) are regarded much attention because of its superior long-term thermal, photochemical stability, low phonon energy [28–30]. Both oxides are isostructural belong to the cubic fluorite structure (Space group *Ia* 3(206)) [31]. Luminescent lanthanide activated Gd_2O_3 NPs exhibited robust charge transfer, good emission lines and shifting of charge transfer band edge towards longer wavelength relatively luminescent rare-earth activated yttrium oxide (Y_2O_3) NPs due to smaller electronegativity, larger atomic radius of the Gd(III) allows an easier charge transfer from the 2p orbital of O_2 to the 4f-orbital of luminescent Eu and Tb metal ions [32–34]. Besides that, the $^8S \rightarrow {}^6D$ (at ~250 nm) and $^8S_{7/2} \rightarrow {}^6IJ$ (at ~270 nm) transitions of Gd(III) overlap the charge transfer band, which greatly improve the emission transition via efficient energy transfer from Gd to luminescent Eu and Tb ions. Furthermore, because of unpaired 4*f* -orbital in Gd(III) exhibited excellent magnetic properties, which is well known for their applications in magnetic resonance imaging(MRI) as a contrast agent [30,31,35–39]. These outstanding photo-physical features make them an ideal matrix for substitution of luminescent metal ions. However, Gd^{3+} ion is related with wide forbidden energy band gap semiconductor and its neighbors Eu^{3+} and

* Corresponding author.
E-mail address: aneesaansari@gmail.com (A.A. Ansari).

https://doi.org/10.1016/j.jphotochem.2018.10.050
Received 10 May 2018; Received in revised form 12 October 2018; Accepted 26 October 2018
Available online 29 October 2018

Tb^{3+} have moderate gaps due to the existence of mid-gap levels. The substitution of Eu(III) and Tb(III) ions into wide energy bandgap semiconductor oxides could offer prominent spectral features with much-improved emission lines and selective 5d-4f transitions with long emission lifetime response [30,40–44].

Up to now, several synthesis routes have been developed for the fabrication of Gd_2O_3 NPs, including combustion, sol-gel chemical, co-precipitation, hydrothermal/solvothermal, microwave, micro-emulsion, thermal decomposition, and surfactant-assisted assembly mechanism etc [1,28,45–48]. All these synthesis methods are well-known and consistently applied for the synthesis of luminescent oxide nanomaterials. Among all these synthesis methods, thermal decomposition process at low temperature is an important technique for the synthesis of low dimension Gd_2O_3 nanostructures [31,34,49–52]. The thermal decomposition process for the synthesis of luminescent NPs has become most attractive due to high purity, low processing temperature, eco-friendly process, homogeneous mixing, uniform, and nearly spherical shaped particles. Besides that, low energy consumption makes them the most suitable technique for large-scale production of luminescent Gd_2O_3 NPs. The Tb-substituted Gd_2O_3 NPs produced vast interest due to their outstanding luminescent properties in the visible region [53–55].

In the present study, we demonstrated the synthesis of Gd_2O_3 NPs using a weak base (urea) based homogeneous co-precipitation process and systematically characterized by different physic-chemical techniques to inspect the photophysical properties of the as-synthesized NPs. Our finding shows the remarkable strong green emission $^5D_4 \rightarrow {}^7F_5$ transition in the middle of a visible region in between 535–560 nm. Here, we presented deeper insight for the understanding colloidal stability, solubility, and biocompatible nature of the as-synthesized luminescent Gd_2O_3:Tb NPs. It is an effort to exploit the 5d-4f mediated optoelectronic properties as well as Raman active modes of cubic structure Gd_2O_3:Tb NPs. It is fact that Tb-mediated NPs are well known for good emission characteristics from $^5D_4 \rightarrow {}^7Fj$ transitions in the visible region. In literature, very few studies were reported and investigated their photophysical properties [56,57]. The main advantage of these non-surfaces modified luminescent NPs are good colloidal solubility in aqueous media, porous structure, excellent biocompatibility, and remarkable luminescent efficiencies could be a future candidate for fluorescent biological applications.

2. Experimental

2.1. Materials

Gd_2O_3(99%, BDH chemicals,UK), Tb_3O_7 (99.99%, Alfa Aesar, Germany), ethanol (E-Merck, Germany), nitric acid and $(NH_2)_2CO$ were utilized as the beginning materials without any assist filtration. Gd $(NO_3)_3 6H_2O$ and Tb$(NO_3)_3 6H_2O$ were prepared by dissolving the corresponding oxides in minimum amount of 1 pH concentrated nitric acid (2 M, 50 ml), which were further diluted with distilled water. Milli-Q (Millipore, Bedford, MA, USA) water was utilized for synthesis and characterization.

2.2. Preparation of Tb-doped gadolinium oxide NPs

For the synthesis of Gd_2O_3:Tb^{3+} NPs ($Gd_{0.95}Tb_{0.05}O_3$), 0.2 M stock solutions of Gd$(NO_3)_3 6H_2O$ and Tb$(NO_3)_3 6H_2O$ were prepared in dist. H_2O. Briefly, 9.5 ml of Gd$(NO_3)_3 6H_2O$ and 0.5 ml of Tb$(NO_3)_3 6H_2O$ were dissolved in 50 ml of dist. water. Then 5 *g* urea dissolved in aqueous solution was introduced into the vigorously mechanically stirred metal nitrates solution at ambient temperature for homogeneous mixing. After that this transparent solution was kept under a refluxed condition at 150 °C for 4 h until complete precipitation [58–62]. On cooling to room temperature, the white precipitates then segregated to the bottom, which was isolated by centrifugation washed with Milli Q H_2O to remove unreacted reactants. The willing sample was dried in an oven at 80 °C for 6 h for advanced characterization.

2.3. Characterization

The crystal structure and phase purity of the powder was checked by X-ray diffraction (XRD) at ambient temperature with the utilize of Rigaku X-ray diffractometer prepared with a Ni channel utilizing Cu Kα (λ = 1.54056 Å) radiations working with 30 kV accelerating voltage, 25 mA current and 5° 2θ/min in the 2θ range 20-80°. Morphology of the sample was assessed employing a field emission transmission electron microscope (FE-TEM) equipped with the energy dispersive x-ray (EDX, JEM-2100 F, JEOL, Japan) working at an accelerating voltage of 200 kV. EDX examination was utilized to confirm the presence of the components. FE-TEM sample was prepared by depositing a drop of colloidal ethanol solution of the luminescent sample onto carbon-coated copper grid through micropipette. Zeta potential of the as-synthesized NPs suspended in water was measured utilizing Zeta Buddies 90 additionally molecule measure analyzer (Brookhaven instruments corporation Holtsville, NY, USA) at temperature 25 °C. Thermogravimetric analysis (TGA) was recorded from the thermogravimetric analyzer (Mettler Toledo, Expository CH-8603 Schwarzenbach, Switzerland) heating rate of 10°/min between room temperature to 800 °C. Infrared spectra were measured on a Perkin-Elmer 580B FTIR spectrometer using KBr pellet procedure within the frequency range from 4000-400 cm^{-1}. KBr pellet was prepared by mixing of very little amount of sample powder for measuring the FTIR spectrum. The UV/Vis absorption spectra were measured from the Perkin-Elmer Lambda-40 spectrophotometer with the sample contained in a 1 cm^3 stopper quartz cell of 1 cm path length in the range 200–600 nm wavelength. Photoluminescence spectra were recorded on Horiba Synapse 1024 × 256 pixels, measure of the pixel: 26 µm, detection range: 300 (effectiveness 30%) to 1000 nm (efficiency:35%). For all estimations, an opening width of 100 µm is utilized, guaranteeing a ghastly determination way better than 1 cm^{-1}.

3. Results and discussion

The synthesis of luminescent NPs via urea-based homogeneous co-precipitation method was first developed by Matijević and his co-workers [63]. Urea is well known the weak base and which is homogeneously decompose in the very slow process with lanthanide metal ions into hydroxyl and carbonate at elevated temperature (~100 °C). XRD pattern was performed to determine the phase purity, crystal structure, and crystallinity of the as-synthesized material. In Fig. 1, diffractogram of Gd_2O_3:Tb NPs display all diffraction planes such as

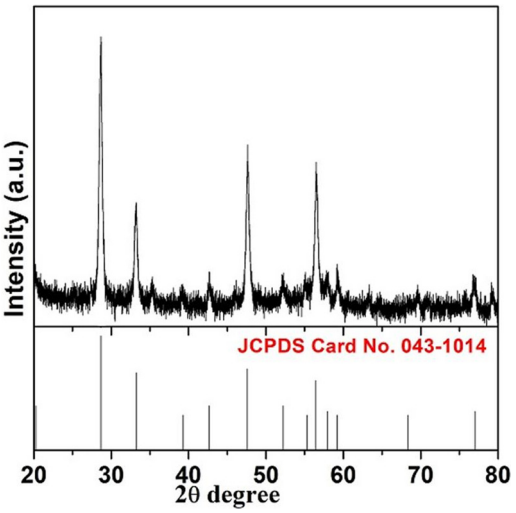

Fig. 1. X-ray diffraction pattern of Gd_2O_3:Tb NPs.

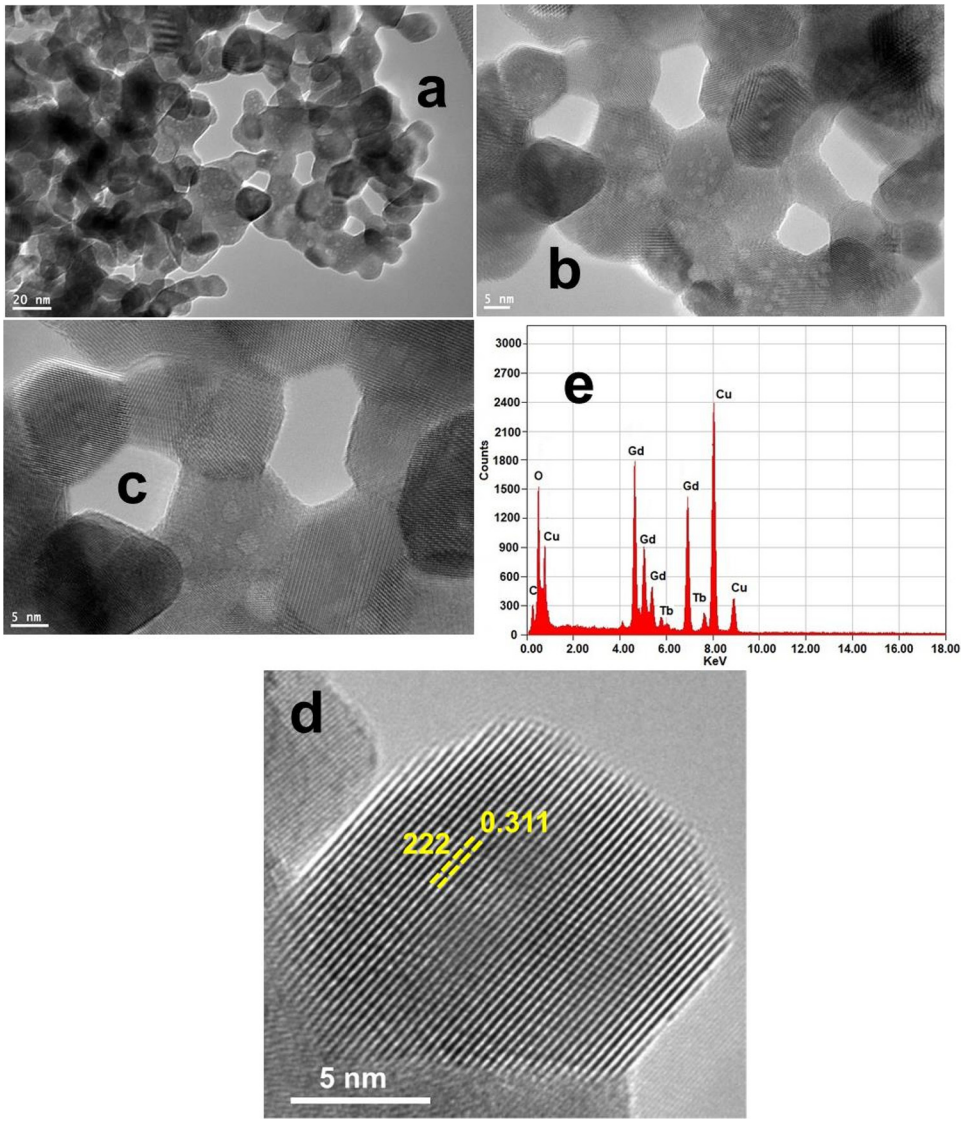

Fig. 2. TEM micrographs of (a) low magnification (b) high magnification (c) High resolution (d) high resolution single particle Gd_2O_3:Tb nanoparticles(f) EDX analysis of the Gd_2O_3:Tb NPs.

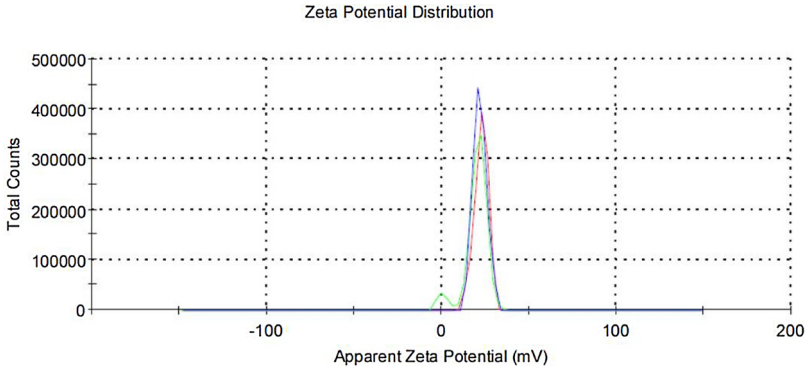

Fig. 3. Zeta potential value of the as-prepared Gd_2O_3:Tb NPs.

(222), (400), (431), (440) and (622), which are closely matched to the pure cubic Gd_2O_3 (JCPDS Card No. 043-1014) [56,64,65]. The reflection lines positions and intensity are perfectly matched with the literature reports. The reflection lines positions and intensified are perfectly coordinated with the previous reports The reflection lines positions and escalated are flawlessly coordinated with the writing reports. No additional peak related to any impurities such as (Tb_2O_3) over the entire XRD pattern is observed, it indicated the phase purity and homogeneous dispersion of the terbium ions into the Gd_2O_3 crystal lattice and formation of Gd-O-Tb solid solution. As illustrate in Fig. 1, the reflection peaks widths are broadened compare to the macro-crystalline materials, it suggests the small grain size with a high crystallinity

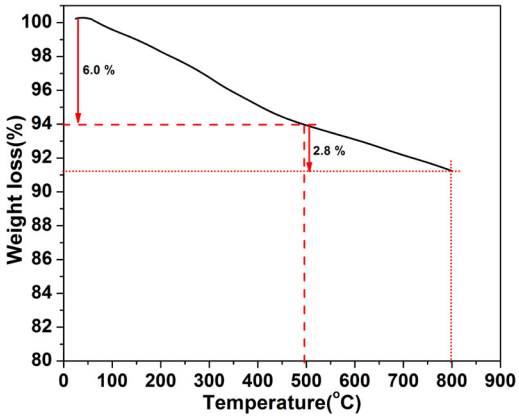

Fig. 4. Thermo-gravimetric analysis of Gd_2O_3:Tb NPs.

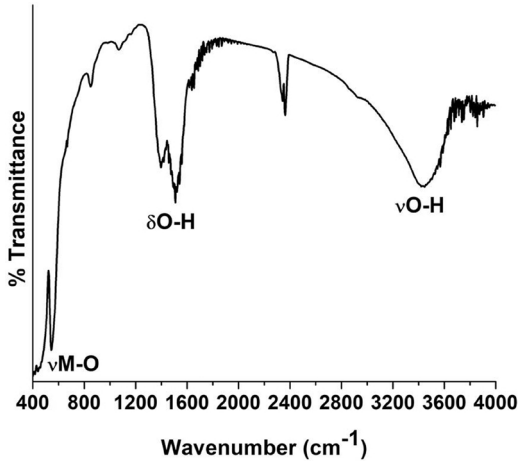

Fig. 5. FTIR spectra of the as-prepared Gd_2O_3:Tb NPs.

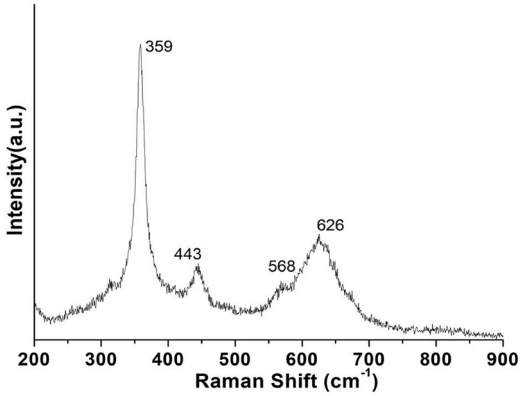

Fig. 6. FT-Raman spectra of the Gd_2O_3:Tb NPs.

of the material. The average grain size of the NPs was estimated from the full-width half maxima (0.46°) of the most dominant peak observed in XRD pattern at $2\theta = 28.67°$ is 15–17 nm.

Morphology of the as-prepared luminescent NPs was inspected from high-resolution transmission electron miscopy. As seen in TEM image Fig. 2a, in the prepared sample NPs are nearly spherical shaped, highly crystalline, rough surface, irregular shape& size, narrow size distribution with an average grain size 10–20 nm, which is in good agreement with the XRD results. Although, the surface of the NPs is fairly irregular greatly porous as seemingly observed in TEM micrographs (Fig. 2c&d). The surface porosity of the luminescent NPs is assisting for the high dispersibility in organic media. As shown in Fig. 2a-c, the luminescent

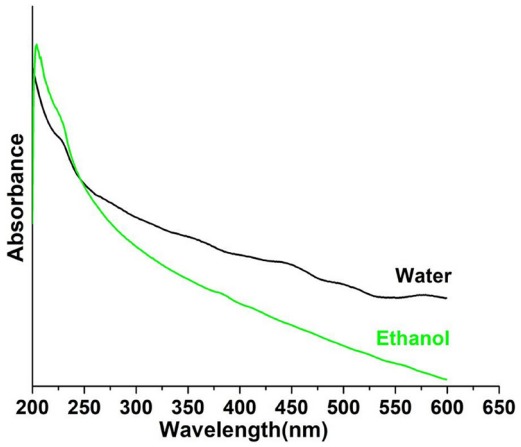

Fig. 7. UV–vis absorption spectra of Gd_2O_3:Tb NPs suspended in dist. water and ethanol.

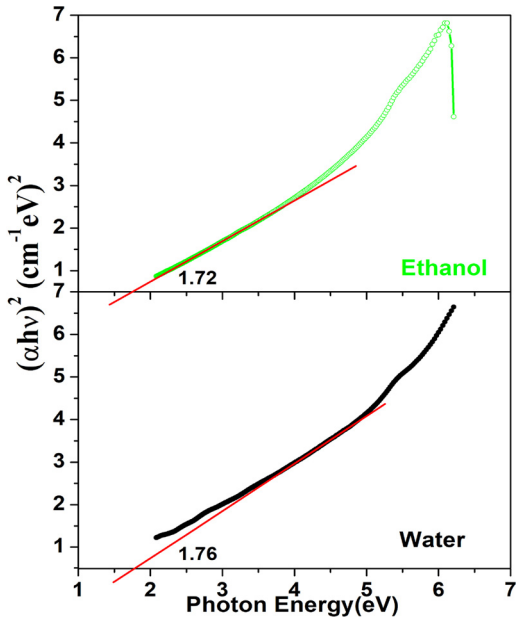

Fig. 8. The plot of $(\alpha h\nu)^2$ vs. photon energy($h\nu$) of the Gd_2O_3:Tb NPs in dist. water and ethanol.

NPs are highly aggregated, it likely due to the rough surface of the NPs, which promises to enhance accumulation process through hydrogen bonding in aqueous media. The higher magnification image in Fig. 2c& d, clearly revealed the lattice fringes with single particle inter-planar spacing of 0.311 nm corresponding to the D-spacing for the (222) crystal lattice plane of the cubic fluorite structure of the Gd_2O_3 material. The chemical composition of the as-prepared luminescent NPs was determined from energy dispersive x-ray analysis (EDX). EDX spectrum in Fig. 2e, illustrates the presence of all expected constituents such as gadolinium (Gd), oxygen (O) and terbium (Tb) ions, indicating the homogeneous distribution inside the crystal matrix. Notably, observed strong peaks of C and Cu are belonging to the carbon-coated copper grid. No other impurity peak is evident over the entire EDX spectrum, it further verified the phase purity of the as-prepared material. Due to rough surface and high porosity of the as-prepared luminescent NPs, the luminescent NPs are hydrophilic in nature and easily dispersed in polar organic solvents such as water and alcohols. After treatment in aqueous media, the luminescent NPs dispersed well and forming a semi-transparent colloidal solution. The observed zeta potential value of the luminescent NPs at physiological pH is 21.7 mV, it endorses the superior

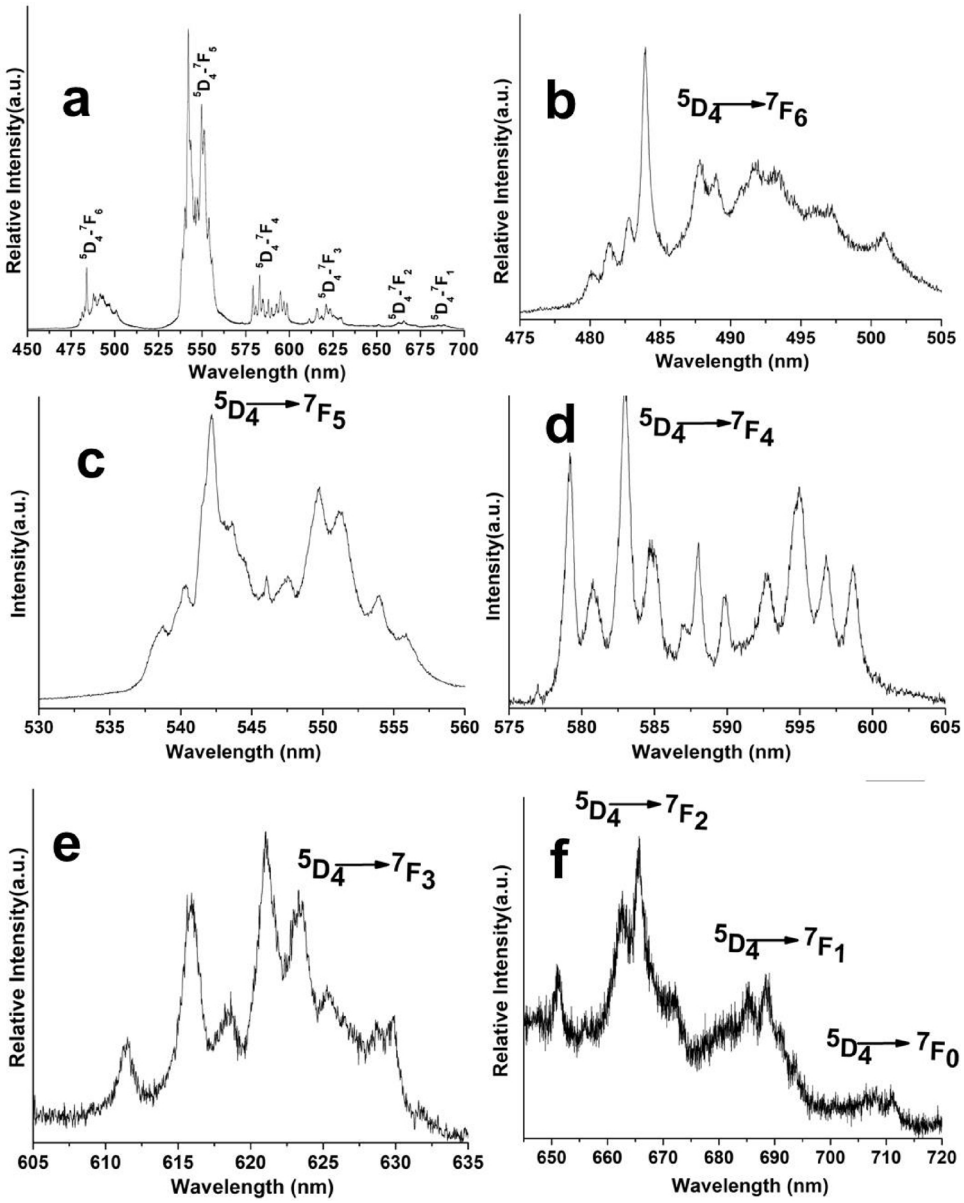

Fig. 9. Photoluminescence spectra of the Gd_2O_3:Tb Ns.

dispersion of the porous luminescent NPs (Fig. 3).

Thermal analysis was performed to certify the phase purity, surface-attached to water molecules or organic moieties and thermal stability of the as-prepared metal oxide. TGA analysis was recorded at room temperature to 800 °C under a nitrogen atmosphere at a heating rate 10 °C/min. As observed in Fig. 4, an exothermic decomposition of the bare NPs proceeded gradually from 100 °C up to 500 °C. The observed weight loss is calculated to be 6%, due to the decomposition of physically surface adsorbed water molecules which are in trace amounts and surface organic moieties. It is well-known fact that, water molecules are generally found in two form first one is in non-crystalline surface adsorbed oxygen vacancies and second one crystalline form or lattice oxygen vacancies. According to the previous literature reports, the lattice oxygen vacancies are decomposed at a higher temperature. The thermogram curve illustrates further continuous weight loss (~2.8%) between 600–800 °C, which is attributed to the burning and removal of dangling bonds and carbon monoxide (Fig. 4). These results are well consistent with FTIR spectral results.

The infrared spectra allow more insight into the surface attached organic moieties of the as-prepared Gd_2O_3:Tb NPs. The occurrence of the diffused band at 3435 cm^{-1} along with middle-intensity peak located at 1510 &1396 cm^{-1} are attributed to the stretching and bending vibrational modes of surface adsorbed residual traces of water molecules (Fig. 5). A sharp intensity infrared absorption peak is observed at 550 cm^{-1} is assigned to the metal oxygen network in the as-prepared Gd_2O_3:Tb NPs [25,54,55,66]. Raman spectroscopy was employed for examining the structural disorder in the as-prepared nanomaterials through Raman-active vibrational modes. The Raman spectrum in Fig. 6 demonstrates three major peaks located at 359, 443 and 626 cm^{-1}. The spectrum shows very strong Raman-active mode located at 359 cm^{-1}, which is a well-known F_g mode for the cubic phase of nanostructured gadolinium oxide (Fig. 6) [36,40,65].

Absorption spectra were recorded in water and alcohol to inspect the optical features and solubility character of the sample over the 200–650 nm UV/visible range. The absorption spectra of Gd_2O_3:Tb NPs in aqueous media exhibited strong absorption in the ultraviolet region, which is attributed to the 5d⟵4f transition [40,56]. Additionally, a small shoulder is observed at 230 nm is assigned to the transition from the ground state of $^8S_{7/2}$ to the excited state of ^{6}Ij for Gd(III) (Fig. 7). In comparative results, ethanol suspended Gd_2O_3:Tb NPs shows good

colloidal stability and solubility then their respective water suspended NPs. We speculate that the high polarity of ethanol is responsible for easily coordinate with porous materials, which make electrostatic interaction through hydrogen bonding. The optical energy band gap was estimated by using the following equation $(\alpha h\nu)^n = \beta(h\nu - E_g)$, where $h\nu$ is the photon energy, α is the absorption coefficient, β is a constant relative to the material, and n is either two for a direct transition or 1/2 for an indirect transition. The intercept of the tangent to the plot will give a worthy estimate of the straight band gap energies of the sample. The experimentally calculated E_g values for H_2O and ethanol are 1.76 and 1.72 eV, respectively (Fig. 8).

Photoluminescence spectra were carried out to confirm the substitution of luminescent Tb(III) ion in the Gd_2O_3 crystal lattice. The emission spectrum of Gd_2O_3:Tb NPs was achieved at an ambient temperature in the middle of the visible region from 450 to 700 nm under monitoring 325 nm(3.82 eV) excitation wavelength. PL spectrum of luminescent NPs in Fig. 9 displays all intra-configurationally emission transitions in visible region located at 480-505($^5D_4 \rightarrow {}^7F_6$), 535-560($^5D_4 \rightarrow {}^7F_5$), 577-600($^5D_4 \rightarrow {}^7F_4$), 610-630($^5D_4 \rightarrow {}^7F_3$), 650-670($^5D_4 \rightarrow {}^7F_2$), 675-700($^5D_4 \rightarrow {}^7F_1$) and 700-715($^5D_4 \rightarrow {}^7F_0$) of terbium ion, respectively [53–55,57]. Among the emission transitions, green region emission transition located at 535-560($^5D_4 \rightarrow {}^7F_5$) is most dominant, which is a so-called hypersensitive transition [56,59,67]. The hypersensitive transition is the true impression of the characteristic 4f-4f transitions, which is induced due to the alteration of surrounding chemical environment through the creation of a new chemical bond between chelate and Tb(III) ions. It is observed in Fig.9, most of the emission lines are highly perturb and display inhomogeneous broadening along with multiple splitting because of crystal field effect. I could be due to small crystallinity and porous surface of the luminescent NPs material. Furthermore, the peak positions are shifted compared to the other Tb^{3+}-doped matrices, since the 4f energy levels of the Tb(III) is shielded by the $5s^2p^6$ outer sub-shell electrons, which affect the crystal field.

4. Conclusion

In summary, Gd_2O_3:Tb NPs were successfully synthesized by thermal decomposition process via a weak base (urea) at low temperature. Luminescent NPs were nearly spherical shaped, narrow size distributed, porous, highly purified, well-crystalline, single cubic phase with an average crystallite size of 10–20 nm. The XRD and Raman active modes result clearly revealed the cubic phase of the luminescent Gd_2O_3:Tb NPs. Because of small grain size and porous surface, the luminescent NPs are hydrophilic in nature and showed aggregated in aqueous media. Optical energy band gap values are varied in both solvents because of polarity and coordination nature of the solvents with luminescent NPs. Our finding of the basic photo-physical features of the as-prepared Gd_2O_3:Tb NPs are highly attractive for future fabrication of large-scale highly efficient nano-phosphors. The highly colloidal luminescent NPs revealed strong green emission transition in between 535–560 nm ($^5D_4 \rightarrow {}^7F_5$) with high thermal and photochemical stability is advantageous in the conjugation of bio-macromolecules for fabrication of optical bio-probe/ optical biosensor.

Acknowledgment

The authors extend their appreciation to the Deanship of Scientific Research, King Saud University, Riyadh, for funding this work through research group No. (RG-1439-089).

References

[1] M.L. Debasu, D. Ananias, A.G. Macedo, J. Rocha, L.D. Carlos, Emission-decay curves, energy-transfer and effective-refractive index in Gd2O3:Eu3+ nanorods, J. Phys. Chem. C 115 (2011) 15297–15303.
[2] S.Y. Hou, Y.C. Zou, X.C. Liu, X.D. Yu, B. Liu, X.J. Sun, Y. Xing, CaF2 and CaF2:Ln (3+) (Ln = Er, Nd, Yb) hierarchical nanoflowers: hydrothermal synthesis and luminescent properties, Crystengcomm 13 (2011) 835–840.
[3] K.A. Abel, H.J. Qiao, J.F. Young, F.C.J.M. van Veggel, Four-fold enhancement of the activation energy for nonradiative decay of excitons in PbSe/CdSe Core/Shell versus PbSe colloidal quantum dots, J. Phys. Chem. Lett. 1 (2010) 2334–2338.
[4] G. Ajithkumar, B. Yoo, D.E. Goral, P.J. Hornsby, A.L. Lin, U. Ladiwala, V.P. Dravid, D.K. Sardar, Multimodal bioimaging using a rare earth doped Gd2O2S:Yb/Er phosphor with upconversion luminescence and magnetic resonance properties, J. Mater. Chem. B 1 (2013) 1561–1572.
[5] T.S. Atabaev, Z. Piao, Y.H. Hwang, H.K. Kim, N.H. Hong, Bifunctional Gd2O3:Er3+ particles with enhanced visible upconversion luminescence, J. Alloys. Compd. 572 (2013) 113–117.
[6] Z. Abbas, S. Dasari, A.K. Patra, Ternary Eu(III) and Tb(III) beta-diketonate complexes containing chalcones: photophysical studies and biological outlook, RSC Adv. 7 (2017) 44272–44281.
[7] A. Bagheri, H. Arandiyan, C. Boyer, M. Lim, Lanthanide-doped upconversion nanoparticles: emerging intelligent light-activated drug delivery systems, Adv. Sci. 3 (2016).
[8] S. Bhattacharyya, M.K. Barman, A. Baidya, A. Patra, Singlet oxygen generation from polymer nanoparticles-photosensitizer conjugates using FRET cascade, J. Phys. Chem. C 118 (2014) 9733–9740.
[9] C.W. Chen, Y.C. Chan, M. Hsiao, R.S. Liu, Plasmon-enhanced photodynamic Cancer therapy by upconversion nanoparticles conjugated with Au nanorods, Acs Appl Mater Inter 8 (2016) 32108–32119.
[10] G.Y. Chen, H. Agren, T.Y. Ohulchanskyy, P.N. Prasad, Light upconverting core-shell nanostructures: nanophotonic control for emerging applications, Chem. Soc. Rev. 44 (2015) 1680–1713.
[11] Q. Chen, C. Wang, L. Cheng, W.W. He, Z. Cheng, Z. Liu, Protein modified upconversion nanoparticles for imaging-guided combined photothermal and photodynamic therapy, Biomaterials 35 (2014) 2915–2923.
[12] V. Agrawal, D. Shahjad, R. Bhardwaj, G.D. Bhargav, R.K. Sharma, A. Bhardwaj, S. Patra, Chand, morphology and doping level of electropolymerized biselenophene-flanked 3,4-Ethylenedioxythiophene polymer: effect of solvents and electrolytes, Electrochim. Acta 192 (2016) 52–60.
[13] G.Y. Chen, J. Damasco, H.L. Qiu, W. Shao, T.Y. Ohulchanskyy, R.R. Valiev, X. Wu, G. Han, Y. Wang, C.H. Yang, H. Agren, P.N. Prasad, Energy-cascaded upconversion in an organic dye-sensitized Core/Shell fluoride nanocrystal, Nano Lett. 15 (2015) 7400–7407.
[14] X. Chen, W. Xu, H.W. Song, C. Chen, H.P. Xia, Y.S. Zhu, D.L. Zhou, S.B. Cui, Q.L. Dai, J.Z. Zhang, Highly efficient LiYF4:Yb3+, Er3+ upconversion single crystal under solar cell Spectrum excitation and photovoltaic application, Acs Appl Mater Inter 8 (2016) 9071–9079.
[15] Z. Chen, H. Jia, X.W. Zhang, J.M. Liu, S.F. Zeng, Y. Li, Z.J. Ma, G.P. Dong, J.R. Qiu, BaCl2:Er(3+)A High Efficient Upconversion Phosphor for Broadband Near-Infrared Photoresponsive Devices, J. Am. Ceram. Soc. 98 (2015) 2508–2513.
[16] S. Dutta, A.K. Patra, S. De, A. Bhaumik, B. Saha, Self-assembled TiO2 nanospheres by using a biopolymer as a template and its optoelectronic application, Acs Appl Mater Inter 4 (2012) 1560–1564.
[17] K.M. Guo, M.Y. Li, X.L. Fang, M.D. Luoshan, L.H. Bai, X.Z. Zhao, Performance enhancement in dye-sensitized solar cells by utilization of a bifunctional layer consisting of core shell beta-NaYF4:Er3+/Yb3+@SiO2 submicron hexagonal prisms, J. Power Sources 249 (2014) 72–78.
[18] M. He, X.C. Pang, X.Q. Liu, B.B. Jiang, Y.J. He, H. Snaith, Z.Q. Lin, Monodisperse dual-functional upconversion nanoparticles enabled near-infrared organolead halide perovskite solar cells, Angew. Chemie Int. Ed. English 55 (2016) 4280–4284.
[19] J.T. Xu, P.P. Yang, M.D. Sun, H.T. Bi, B. Liu, D. Yang, S.L. Gai, F. He, J. Lin, Highly emissive dye-sensitized upconversion nanostructure for dual-photosensitizer photodynamic therapy and bioimaging, ACS Nano 11 (2017) 4133–4144.
[20] L.L. Feng, S.L. Gai, F. He, Y.L. Dai, C.N. Zhong, P.P. Yang, J. Lin, Multifunctional mesoporous ZrO2 encapsulated upconversion nanoparticles for mild NIR light activated synergistic cancer therapy, Biomaterials 147 (2017) 39–52.
[21] L.L. Feng, F. He, B. Liu, G.X. Yang, S.L. Gai, P.P. Yang, C.X. Li, Y.L. Dai, R.C. Lv, J. Lin, G-C3N4 coated upconversion nanoparticles for 808 nm near-infrared light triggered phototherapy and multiple imaging, Chem. Mater. 28 (2016) 7935–7946.
[22] K.A. Abel, P.A. FitzGerald, T.Y. Wang, T.Z. Regier, M. Raudsepp, S.P. Ringer, G.G. Warr, F.C.J.M. van Veggel, Probing the structure of colloidal Core/Shell quantum dots formed by cation exchange, J. Phys. Chem. C 116 (2012) 3968–3978.
[23] P. Haro-Gonzalez, P.R. Sevilla, F. Sanz-Rodriguez, E.M. Rodriguez, N. Bogdan, J.A. Capobianco, K. Dholakia, D. Jaque, Gold nanorod assisted intracellular optical manipulation of silica microspheres, Opt. Express 22 (2014).
[24] B. Jana, S. Bhattacharyya, A. Patra, Conjugated polymer P3HT-Au hybrid nanostructures for enhancing photocatalytic activity, Phys. Chem. Chem. Phys. 17 (2015) 15392–15399.
[25] A.A. Ansari, M. Alam, J.P. Labis, S.A. Alrokayan, G. Shafi, T.N. Hasan, N.A. Syed, A.A. Alshatwi, Luminescent mesoporous LaVO4:Eu3+ core-shell nanoparticles: synthesis, characterization, biocompatibility and their cytotoxicity, J. Mater. Chem. 21 (2011) 19310–19316.
[26] A.A. Ansari, J.P. Labis, Preparation and photoluminescence properties of hydrothermally synthesized YVO4:Eu3+ nanofibers, Mater. Lett. 88 (2012) 152–155.
[27] A.A. Ansari, J.P. Labis, M.A. Manthrammel, Designing of luminescent GdPO4:Eu@LaPO4@SiO2 core/shell nanorods: synthesis, structural and luminescence properties, Solid State Sci. 71 (2017) 117–122.
[28] J. Fang, P. Chandrasekharan, X.L. Liu, Y. Yang, Y.B. Lv, C.T. Yang, J. Ding, Manipulating the surface coating of ultra-small Gd2O3 nanoparticles for improved T-1-weighted MR imaging, Biomaterials 35 (2014) 1636–1642.

[29] C.C. Huang, C.H. Su, W.M. Li, T.Y. Liu, J.H. Chen, C.S. Yeh, Bifunctional Gd2O3/C nanoshells for MR imaging and NIR therapeutic applications, Adv. Funct. Mater. 19 (2009) 249–258.
[30] I.F. Li, C.H. Su, H.S. Sheu, H.C. Chiu, Y.W. Lo, W.T. Lin, J.H. Chen, C.S. Yeh, Gd2O (CO3)(2)center dot H2O particles and the corresponding Gd2O3: synthesis and applications of magnetic resonance contrast agents and template particles for hollow spheres and hybrid composites, Adv. Funct. Mater. 18 (2008) 766–776.
[31] C.C. Huang, T.Y. Liu, C.H. Su, Y.W. Lo, J.H. Chen, C.S. Yeh, Superparamagnetic hollow and paramagnetic porous Gd2O3 particles, Chem. Mater. 20 (2008) 3840–3848.
[32] H.J. Lee, J.U. Park, S. Choi, J. Son, M. Oh, Synthesis and Photoluminescence Properties of Eu3+-Doped Silica@Coordination Polymer CoreShell Structures and Their Calcinated Silica@Gd2O3:Eu and Hollow Gd(2O)3:Eu Microsphere Products, Small 9 (2013) 561–569.
[33] G.G. Li, C. Peng, C.X. Li, P.A.P. Yang, Z.Y. Hou, Y. Fan, Z.Y. Cheng, J. Lin, Shape-controllable synthesis and morphology-dependent luminescence properties of GaOOH:Dy3+ and beta-Ga2O3:Dy3+, Inorg. Chem. 49 (2010) 1449–1457.
[34] J.G. Li, Q. Zhu, X.D. Li, X.D. Sun, Y. Sakka, Colloidal processing of Gd2O3:Eu3+ red phosphor monospheres of tunable sizes: solvent effects on precipitation kinetics and photoluminescence properties of the oxides, Acta Mater. 59 (2011) 3688–3696.
[35] K.H. Lee, B.I. Lee, J.H. You, S.H. Byeon, Transparent Gd2O3 : Eu phosphor layer derived from exfoliated layered gadolinium hydroxide nanosheets, Chem. Commun. (Camb.) 46 (2010) 1461–1463.
[36] B. Antic, J. Rogan, A. Kremenovic, A.S. Nikolic, M. Vucinic-Vasic, D.K. Bozanic, G.F. Goya, P. Colomban, Optimization of photoluminescence of Y2O3:Eu and Gd2O3:Eu phosphors synthesized by thermolysis of 2,4-pentanedione complexes, Nanotechnology 21 (2010).
[37] W. Ge, Z. Li, Z.W. Lei, T. Chen, Z.P. Fu, R.R. Peng, M. Liu, Y.L. Lu, Synthesis of hexagonal phase Gd2O2CO3:Yb3+, Er3+ upconversion nanoparticles via SiO2 coating and Nd3+ doping, Crystengcomm 17 (2015) 5702–5709.
[38] A. Jain, G.A. Hirata, M.H. Farias, F.F. Castillon, Synthesis and characterization of (3-Aminopropyl)trimethoxy-silane (APTMS) functionalized Gd2O3:Eu3+ red phosphor with enhanced quantum yield, Nanotechnology 27 (2016).
[39] G. Jia, H.P. You, K. Liu, Y.H. Zheng, N. Guo, H.J. Zhang, Highly uniform Gd2O3 hollow microspheres: template-directed synthesis and luminescence properties, Langmuir 26 (2010) 5122–5128.
[40] J.G. Kang, B.K. Min, Y. Sohn, Synthesis and characterization of Gd(OH)(3) and Gd2O3 nanorods, Ceram. Int. 41 (2015) 1243–1248.
[41] J.H. Kim, Y.K. Jung, J.K. Lee, Synthesis and characterization of hollow nano-particles of crystalline Gd2O3, J. Nanoparticle Res. 13 (2011) 2311–2318.
[42] A. Kumar, S.P. Tiwari, A.K. Singh, K. Kumar, Synthesis of Gd2O3:Ho3+/Yb3+ upconversion nanoparticles for latent fingermark detection on difficult surfaces, Appl Phys B-Lasers O 122 (2016).
[43] R.M. Li, L. Li, Y.H. Han, S.L. Gai, F. He, P.P. Yang, Core-shell structured Gd2O3: Ln@mSiO(2) hollow nanospheres: synthesis, photoluminescence and drug release properties, J. Mater. Chem. B 2 (2014) 2127–2135.
[44] R.S. Ningthoujam, R. Shukla, R.K. Vatsa, V. Duppel, L. Kienle, A.K. Tyagi, Gd2O3:Eu3+ particles prepared by glycine-nitrate combustion: phase, concentration, annealing, and luminescence studies, J. Appl. Phys. 105 (2009).
[45] D.H. Chavez, O.E. Contreras, G.A. Hirata, Synthesis and upconversion luminescence of nanoparticles Y2O3 and Gd2O3 Co-doped with Yb3+ and Er3+, Nanomater. Nanotechnol. 6 (2016).
[46] S.L. Gai, P.P. Yang, D. Wang, C.X. Li, N. Niu, F. He, X.B. Li, Monodisperse Gd2O3:Ln (Ln = Eu3+, Tb3+, Dy3+, Sm3+, Yb3+/Er3+, Yb3+/Tm3+, and Yb3+/Ho3+) nanocrystals with tunable size and multicolor luminescent properties, Crystengcomm 13 (2011) 5480–5487.
[47] J. Huang, Y.H. Song, G.W. Wang, Y. Sheng, K.Y. Zheng, H.B. Li, H.G. Zhang, Q.S. Huo, X.C. Xu, H.F. Zou, Surfactant-assisted synthesis and luminescent properties of Gd2O3:Eu3+ core-shell microspheres, J. Alloys. Compd. 574 (2013) 310–315.
[48] L.G. Jacobsohn, B.L. Bennett, R.E. Muenchausen, S.C. Tornga, J.D. Thompson, O. Ugurlu, D.W. Cooke, A.L.L. Sharma, Multifunction Gd2O3 : Eu nanocrystals produced by solution combustion synthesis: structural, luminescent, and magnetic characterization, J. Appl. Phys. 103 (2008).
[49] G. Cheng, J.L. Zhang, Y.L. Liu, D.H. Sun, J.Z. Ni, Monodisperse REPO4 (RE = Yb, Gd, Y) hollow microspheres covered with Nanothorns as affinity probes for selectively capturing and labeling phosphopeptides, Chem. Eur. J. 18 (2012) 2014–2020.
[50] G. Jia, M. Yang, Y.H. Song, H.P. You, H.J. Zhang, General and Facile Method To Prepare Uniform Y2O3:Eu Hollow Microspheres, Cryst. Growth Des. 9 (2009) 301–307.
[51] X.L. Jiang, L. Yu, C. Yao, F.Q. Zhang, J. Zhang, C.J. Li, Synthesis and characterization of Gd2O3 hollow microspheres using a template-directed method, Materials 9 (2016).
[52] H.F. Jiu, W.B. Jia, L.X. Zhang, C.S. Huang, Y.J. Feng, Q. Cheng, The synthesis and photoluminescence property of YPO4:Eu3+ hollow microspheres, Superlattices Microstruct. 79 (2015) 9–14.
[53] A.A. Ansari, J. Labis, A.S. Aldwayyan, M. Hezam, Facile synthesis of water-soluble luminescent mesoporous Tb(OH)(3)@SiO2 core-shell nanospheres, Nanoscale Res. Lett. 8 (2013) 1–8.
[54] A.A. Ansari, J.P. Labis, One-pot synthesis and photoluminescence properties of luminescent functionalized mesoporous SiO2@Tb(OH)(3) core-shell nanospheres, J. Mater. Chem. 22 (2012) 16649–16656.
[55] A.A. Ansari, A.K. Parchur, M. Alam, A. Azzeer, Structural and photoluminescence properties of Tb-doped CaMoO4 nanoparticles with sequential surface coatings, Mater. Chem. Phys. 147 (2014) 715–721.
[56] S. Seo, H. Yang, P.H. Holloway, Controlled shape growth of Eu- or Tb-doped luminescent Gd2O3 colloidal nanocrystals, J Colloid Interf Sci 331 (2009) 236–242.
[57] P.F. Du, L.X. Song, J. Xiong, Z.Q. Xi, D.L. Jin, L.C. Wang, Preparation and the luminescent properties of Tb3+-doped Gd2O3 fluorescent nanofibers via electrospinning, Nanotechnology 22 (2011).
[58] W.H. Di, X.G. Ren, L.G. Zhang, C.X. Liu, S.Z. Lu, A facile template-free route to fabricate highly luminescent mesoporous gadolinium oxides, Crystengcomm 13 (2011) 4831–4833.
[59] Y.H. Song, H.P. You, Y.J. Huang, M. Yang, Y.H. Zheng, L.H. Zhang, N. Guo, Highly Uniform and Monodisperse Gd2O2S:Ln(3+) (Ln = Eu, Tb) Submicrospheres: Solvothermal Synthesis and Luminescence Properties, Inorg. Chem. 49 (2010) 11499–11504.
[60] C.B. Tan, Y.X. Liu, W.B. Li, Y.T. Zhang, Y.N. Han, Uniform lanthanide-doped Y2O3 hollow microspheres: controlled synthesis and luminescence properties, Mater Sci Eng B-Adv 176 (2011) 1251–1256.
[61] J. Yang, Z.W. Quan, D.Y. Kong, X.M. Liu, J. Lin, Y2O3 : Eu3+ microspheres: solvothermal synthesis and luminescence properties, Cryst. Growth Des. 7 (2007) 730–735.
[62] P.P. Yang, S.L. Gai, Y.C. Liu, W.X. Wang, C.X. Li, J. Lin, Uniform hollow Lu2O3:ln (Ln = Eu3+, Tb3+) spheres: facile synthesis and luminescent properties, Inorg. Chem. 50 (2011) 2182–2190.
[63] E. Matijevic, W.P. Hsu, Preparation and properties of monodispersed colloidal particles of lanthanide compounds .1. gadolinium, europium, terbium, samarium, and cerium(Iii), J Colloid Interf Sci 118 (1987) 506–523.
[64] T.K. Tseng, J. Choi, M. Davidson, P.H. Holloway, Synthesis and luminescent characteristics of europium dopants in SiO2/Gd2O3 core/shell scintillating nanoparticles, J. Mater. Chem. 20 (2010) 6111–6115.
[65] N. Paul, D. Mohanta, Evaluation of optoelectronic response and Raman active modes in Tb3+ and Eu3+-doped gadolinium oxide (Gd2O3) nanoparticle systems, Appl Phys a-Mater 122 (2016).
[66] A.A. Ansari, A.K. Parchur, M. Alam, A. Azzeer, Effect of surface coating on optical properties of Eu3+-doped CaMoO4 nanoparticles, Spectrochim. Acta A. 131 (2014) 30–36.
[67] C. Louis, R. Bazzi, C.A. Marquette, J.L. Bridot, S. Roux, G. Ledoux, B. Mercier, L. Blum, P. Perriat, O. Tillement, Nanosized hybrid particles with double luminescence for biological labeling, Chem. Mater. 17 (2005) 1673–1682.